MOLECULAR PHYSICS, 10 JUNE 2003, VOL. 101, NO. 11, 1651–1658

Taylor & Francis
Taylor & Francis Group

Laser-induced condensation in colloid–polymer mixtures

INGO O. GÖTZE[1], JOSEPH M. BRADER[2]†,
MATTHIAS SCHMIDT[1]* and HARTMUT LÖWEN[1]

[1] Institut für Theoretische Physik II, Heinrich-Heine-Universität Düsseldorf, D-40225 Düsseldorf, Germany

[2]The James Franck Institute, University of Chicago, South Ellis Ave 5640, Chicago, Il 60637, USA

(*Received 11 October 2002; accepted 22 November 2002*)

We study a mixture of hard sphere colloidal particles and non-adsorbing polymers exposed to a plane wave external potential which represents a three-dimensional standing laser field. With computer simulations and density functional theory we investigate the structure and phase behaviour using the simple Asakura–Oosawa model. For varying laser wavelength λ we monitor the emergence of structure in response to the external field, as measured by the amplitude of the oscillations in the one-body density distribution. Between the ideal gas limit for small λ and the bulk limit of large λ there is a non-monotonic crossover that is governed by commensurability of λ and the colloid diameter. The theoretical curves are in good agreement with simulation results. Furthermore, the effect of the periodic field on the liquid–vapour transition is studied, a situation that we refer to as laser-induced condensation. Above a threshold value for λ the theoretical phase diagram indicates the stability of a 'stacked' fluid phase, which is a periodic succession (in the beam direction) of liquid and vapour slabs. This partially condensed phase causes a splitting of the liquid–vapour binodal leading to two critical and a triple point. All our predictions should be experimentally observable for colloid–polymer mixtures in an optical resonator.

1. Introduction

When a non-adsorbing polymer is added to a sterically-stabilized colloidal dispersion of spherical particles, an effective attraction between the colloids is generated via the depletion mechanism. This mechanism can be understood qualitatively as follows. Each colloidal particle is surrounded by a polymer depletion zone due to the repulsion between the colloidal surface and the polymer. Close to colloidal contact, two depletion zones overlap, such that the polymers have more accessible volume, i.e. their entropy increases. As a consequence, two colloidal particles effectively attract. The depletion attraction was first studied and explained in a simple model of non-interacting polymers by Asakura and Oosawa (AO) in 1958 [1], and later independently by Vrij [2]. In their model, the colloid–polymer interaction is hard-sphere like with a range $R_c + R_p$ larger than the colloidal radius R_c, where R_p is the radius of gyration of the polymer coils [3]. By integrating out the polymeric degrees of freedom [4–6], an analytical form of the attraction is obtained. One lesson to be learned from this expression is that both the range and the depth of the attraction can be tuned by changing the molecular weight and the concentration of the polymers [7, 8].

The effective attraction causes fluid–fluid demixing of the colloids into a colloid-rich (liquid) and colloid-poor (vapour) phase above a critical polymer concentration. A full quantitative understanding of the demixing transition is meanwhile available and experimental data for fluid–fluid phase coexistence are well understood by theory and simulation. What is less clear in the bulk are kinetics from metastable states as well as the gel and glass transition (for a recent review see [9]).

If colloidal dispersions are exposed to an external field, a wealth of new phenomena occur both in equilibrium and non-equilibrium (for a recent review see [10]). One simple possibility for an external field is a hard planar system wall where the AO model of colloid–polymer mixtures was investigated recently. Building on Rosenfeld's ideas [11] a density-functional theory (DFT) for the AO model [12, 13] was proposed and near fluid–fluid coexistence, a novel scenario of *entropic* wetting and a finite sequence of layering transitions was found [14, 15]. This scenario was recently con-

* Author for correspondence. e-mail: mschmidt@thphy.uni-duesseldorf.de. Present address: Soft Condensed Matter, Debye Institut, Utrecht University, Princetonpln 5, 3584 CC Utrecht, The Netherlands.

† Present address: Institute of Physiology, University of Bern, Buehlplatz 5, 3012 Bern, Switzerland.

Molecular Physics ISSN 0026–8976 print/ISSN 1362–3028 online © 2003 Taylor & Francis Ltd
http://www.tandf.co.uk/journals
DOI: 10.1080/0026897031000075651

firmed by computer simulations [16], and there exists also experimental indications [17, 18].

In this paper we study a different kind of external field which can be easily realized in experiments, namely a laser-optical field. This establishes a periodic external potential acting on the colloids of the form

$$U_{\text{ext}}(z) = U_0 \cos(2\pi z/\lambda), \tag{1}$$

where U_0 is the amplitude, λ is the wavelength and z is the spatial coordinate in the beam direction. Research is very active for the freezing transition in similar periodically modulated external potentials (so-called laser-induced freezing). Most of the studies have been done in two dimensions and with mutually repelling colloidal particles. Simultaneously, experiments [19–22], computer simulations [23–25] and theories such as density functional approaches of freezing [26–28] and phenomenological elastic theory [29, 30] have been developed recently. The most striking results are re-entrant melting transitions for increasing U_0 and novel hexatic-type intermediate phases.

However, to the best of our knowledge, a system with attractive interactions—such as the effective attraction generated in a colloid–polymer mixture—has not yet been studied in an external periodic field. This is the aim of the present paper, where we consider a fluid colloid–polymer mixture in an oscillatory potential. We investigate the density profiles caused by the external field, both far away and close to the bulk fluid–fluid phase separation and study them, in particular, as a function of the wavelength λ of the external field (equation (1)) for fixed average densities of both species. Since λ and the particle radii, R_c and R_p, are competing length scales of the problem, interesting behaviour can be expected as one of these variables is changed. For fixed size ratio R_p/R_c we find that there are marked oscillations of the density peak heights as a function of λ provided λ is smaller than about twice the colloid diameter σ_c. These oscillations reflect possible commensurability of λ and σ_c. For λ larger than about $2\sigma_c$, on the other hand, the colloidal density peak height *increases* monotonically with increasing λ. This is in contrast to a polymer-free colloidal system (hard spheres) where the density peak height *decreases* with increasing λ. As explained in detail below these results stem from computer simulations and a recent DFT. In general, we find good agreement between both approaches, hence we trust the theory to correctly describe the system.

Furthermore, we study the bulk liquid–vapour transition in the presence of the external potential (1). It is expected that the presence of the external field will change the phase diagram qualitatively, an effect that we anticipate as *laser-induced condensation*, in analogy with laser-induced freezing in the case of the liquid–solid transition in a periodic field. The theoretical results for the phase diagram show a splitting of the colloid liquid–vapour binodal. In the colloid chemical potential versus polymer reservoir density representation, an unusual (for fluid states) shaped coexistence curve results, resembling an inverted letter *y*. It features two critical points, one between colloid vapour and a novel phase, the stacked fluid; the other is between stacked fluid and colloid liquid. Naturally, we find a triple point where colloid vapour, colloid liquid and the stacked fluid coexist. It is argued that upon decreasing λ the two critical points merge into a bicritical point. Below the corresponding *finite* value of λ the stacked phase ceases to exist and a single liquid–vapour binodal is recovered.

The paper is organized as follows: in § 2 we describe the AO model in an external laser field. The simulation method and the density functional technique are described in § 3 and § 4, respectively. Results for the density profiles and the phase behaviour are presented and discussed in § 5. We conclude in § 6.

2. The model

The AO model is a simple idealized model for colloid–polymer mixtures, where the colloids are treated as hard spheres with a diameter $\sigma_c = 2R_c$, and the polymers as interpenetrating, non-interacting particles. The polymers are excluded by a centre-of-mass distance of $(\sigma_c + \sigma_p)/2$ from the colloids, where $\sigma_p = 2R_p$ with R_p the radius of gyration of the polymer. The number of colloids is denoted by N_c, the number of polymers by N_p and the total volume of the sample by V.

In detail, the pair interaction potentials $U_{ij}(r)$ between species $i, j = c, p$ as a function of the centre-to-centre distance r are given by

$$U_{cc}(r) = \begin{cases} \infty, & \text{for } r < \sigma_c, \\ 0, & \text{otherwise,} \end{cases} \tag{2}$$

$$U_{cp}(r) = \begin{cases} \infty, & \text{for } r < R_c + R_p, \\ 0 & \text{otherwise,} \end{cases} \tag{3}$$

$$U_{pp}(r) = 0. \tag{4}$$

Furthermore we consider the external potential $U_{\text{ext}}(z)$ given in equation (1) acting only on the colloids. No external potential is applied directly to the polymers.

Thermodynamic parameters are the packing fractions $\eta_i = \pi N_i \sigma_i^3/(6V) = \pi \sigma_i^3 \rho_i/6$ of species $i = c, p$, and we also use the packing fraction η_p^r in an ideal reservoir of polymers that is in chemical equilibrium with the system. The size ratios $q = \sigma_p/\sigma_c$ and λ/σ_c and the strength (relative to the thermal energy) of the external

potential βU_0 are control parameters, where $\beta = 1/(k_B T)$, k_B is the Boltzmann constant and T is absolute temperature.

By integrating out the polymer degrees of freedom the binary AO model can be mapped onto a one-component model with effective interactions [4]. Truncating at the two-body level one arrives at the familiar AO potential. If the distance r of two colloids is smaller than $\sigma_c + \sigma_p$, the polymers are excluded from a region between them, so that the osmotic pressure of the polymers on the opposite sides of the colloids is not compensated, and an effective depletion attraction between colloids is induced. The effective potential $U_{AO}(r)$ between colloids is proportional to the overlap-volume of the excluded volumes [1]:

$$U_{AO}(r) = \begin{cases} \infty, & \text{for } r \leqslant \sigma_c, \\ -\Pi_p V_{\text{overlap}}(r), & \text{for } \sigma_c < r \leqslant \sigma_c + \sigma_p, \\ 0, & \text{otherwise,} \end{cases} \tag{5}$$

where $\Pi_p = \rho_p^r k_B T$ is the osmotic pressure of the polymers, where ρ_p^r is the number density in the polymer reservoir. The pairwise overlap-volume V_{overlap} for $\sigma_c < r \leqslant \sigma_c + \sigma_p$ is given by

$$V_{\text{overlap}}(r) = \left(1 - \frac{3r}{2\sigma_c(1+q)} + \frac{1}{2}\left[\frac{r}{\sigma_c(1+q)}\right]^3\right)\frac{\pi}{6}\sigma_c^3(1+q)^3. \tag{6}$$

The effective potential (5) with (6) can be used to treat the mixture as a one-component system with pairwise interactions. This mapping is exact for $q < (2/3^{1/2} - 1) = 0.1547\ldots$, where for geometrical reasons only pairwise overlaps occur. When q is above this threshold, there occur higher-body terms, and using only the pairwise contribution is an approximation.

3. Computer simulation method

In order to treat the full model we perform direct Monte Carlo (MC) simulations of the binary mixture, i.e. besides the colloids, we also simulate the polymers explicitly. This is potentially difficult due to the typically large number of polymers, but still possible as the polymers are non-interacting. Using N_c colloids and N_p polymers, the simulation time scales with N_c^2 and $N_c N_p$ (not with N_p^2 due to polymer ideality). Of course, an advantage of the hard interactions is that it is not necessary to calculate the energy; one only needs to check for overlap of particles. If the moved particles overlap with one other, the configuration is rejected, so the search for further overlaps can be aborted. As the colloid–colloid interaction and the colloid–polymer interaction have different ranges, we employ two Verlet neighbour lists with different Verlet radii in order to optimize the number of particles in each list. We use straightforward canonical simulations, hence fix the numbers of colloids and polymers explicitly. This is easier than (semi-)grandcanonical methods, because inserting additional colloids is prohibited by the polymers, filling the space between the colloids. As we fix η_p in the system, η_p^r is not known *a priori*. This is determined during the simulation by the acceptance probability of inserting (homogeneously distributed) test polymers.

We also perform MC simulations of the effective one-component system of colloids employing only two-body interactions (equations (5) and (6)). These are much faster than the direct simulations of the binary system. As we are interested in $q > 0.1547$, where many-body terms arise in the effective potential, we can quantitatively assess the effect of the higher-order terms by comparing with the direct simulation. The strength of the attraction in the AO pair potential (equation (5)) is ruled by η_p^r. In order to compare with the results from the direct simulation we need to prescribe this value. We do this using the accurate free-volume expression [31].

In more detail, for a given state point we chose corresponding particle numbers of colloids and polymers, $N_c = 300$ and $N_p = 0$, 1500, 3000, respectively, as well as the system volume $V = 1500\sigma_c^3$. We match the box length L_z to be an integer multiple of the wavelength λ, and set the box volume to $V = L_x \times L_y \times L_z$, where L_γ are the box lengths in space direction γ, and $L_x = L_y$. Periodic boundary conditions are used in all three space directions. In the range $\sigma_c \leqslant \lambda \leqslant 7.5\sigma_c$ we use $L_z = 4\lambda$. For $0.25\sigma_c \leqslant \lambda \leqslant 1.25\sigma_c$ we set $L_z = 12\lambda$, in order to avoid finite size effects in the z direction for these smaller λ values.

In the direct simulation we use 5×10^6 MC cycles to equilibrate the system, and typically 2.5–5×10^7 cycles to gather statistics, where one MC cycle consists of one trial move per particle. In the simulation of the effective one-component system the maximum displacement per move can be chosen larger than in the direct simulation, so that less MC cycles are necessary. Here we use 10^6 MC cycles to equilibrate the system, and 10^7 cycles to gather statistics.

4. Density functional theory

In order to study the AO model in an external potential in the framework of DFT one considers the grand potential Ω as a functional of the one-particle density fields $\rho_c(\mathbf{r}), \rho_p(\mathbf{r})$. This is given as

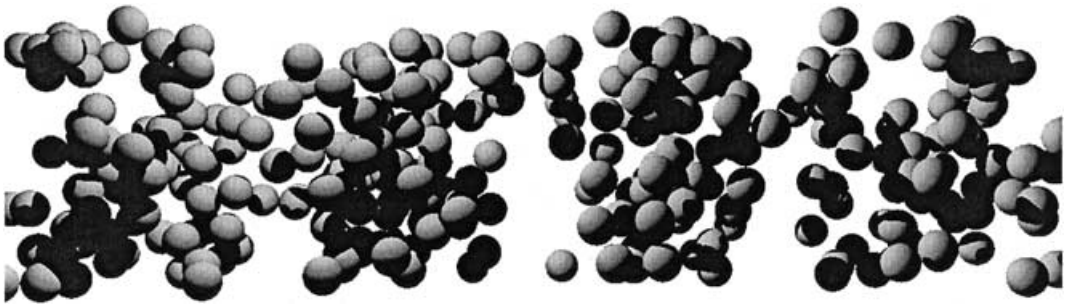

Figure 1. Snapshot of a colloid particle configuration from computer simulation. The polymers are not shown for clarity. The laser beam is along the horizontal direction in the paper plane. Four wavelengths λ are shown, corresponding to figure 2.

$$\beta\Omega[\rho_c(\mathbf{r}),\rho_p(\mathbf{r})] = \sum_{i=c,p}\int d^3r\rho_i(\mathbf{r})[\ln(\rho_i(\mathbf{r})\Lambda_i^3) - 1 - \beta\mu_i] + \beta F_{exc}[\rho_c(\mathbf{r}),\rho_p(\mathbf{r})] + \int d^3r\rho_c(\mathbf{r})\beta U_{ext}(\mathbf{r}), \quad (7)$$

where Λ_i is the (irrelevant) thermal wavelength and μ_i is the chemical potential of species i. The excess (over ideal gas) Helmholtz free energy F_{exc} arises from interactions between particles and is in general (and in the present case of the AO model) unknown. The crucial benefit of DFT is that F_{exc} is expressed as a functional only of the density profile(s), and that it does not explicitly depend on the external potential(s). This allows one to study different external potentials using the *same* prescription for the excess free energy functional.

Relying on an approximation, we use in the following the fundamental measure DFT for the binary AO model developed in [12, 13]. Here we do not report the details of the approximation; the interested reader is referred directly to [12, 13]. The theory was shown to give the same bulk fluid free energy and hence the same fluid demixing curve as free-volume theory [31], which was recently shown by computer simulations to be remarkably accurate for the AO model [32]. Concerning inhomogeneous situations, both fluid–fluid interfaces and wall adsorption have been considered [14, 15].†

5. Results

5.1. *Structure*

Fluid–fluid demixing is stable with respect to fluid–solid for size ratios of (about) $q \geqslant 0.35$ [33]. As we are interested primarily in fluid states we stay above this threshold and consider in the following $q = 0.6$. As a typical value for the strength of the external field we chose $\beta U_0 = 1/2$, hence the difference between minima and maxima of the potential energy is k_BT.

The prominent effect of the plane wave external potential $U_{ext}(z)$ (equation (1)) on the structure is to generate wave-like (non-decaying) one-body distributions $\rho_i(z)$ of both species. To exemplify this (rather straightforward) effect, we show in figure 1 a snapshot and in figure 2 typical results from our computer simulations. The simulation box accommodates four wavelengths of the external potential $U_{ext}(z)$ (upper panel in figure 2). In response to this influence the colloid profile $\rho_c(z)$ exhibits an 'out-of-phase' behaviour, i.e. its maxima coincide with the minima of $U_{ext}(z)$ and vice versa (see the clustering of particles in figure 1). Of course, this effect occurs already without polymers, i.e. in the pure hard sphere case. The density distribution of added polymers, however, is again *in-phase* with $U_{ext}(z)$. This is expected as the external potential does

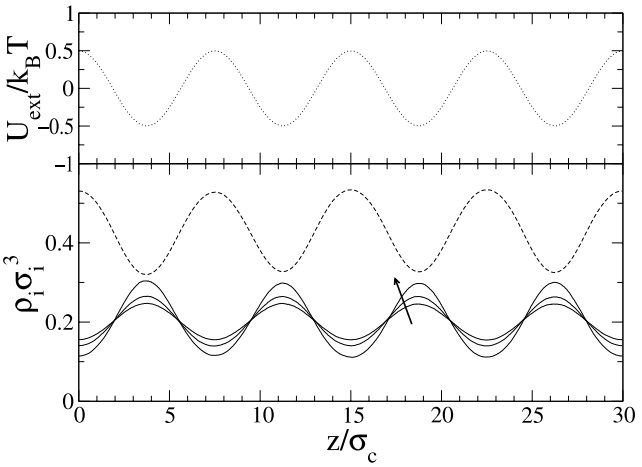

Figure 2. External potential $U_{ext}(z)$ as a function of z/σ_c (upper panel) and corresponding density profiles $\rho_i(z)$ (lower panel) of colloids (solid lines) and polymers (dashed line) for $\lambda = 7.5\sigma_c$. Average densities are $\rho_c\sigma_c^3 = 0.2$ and increasing $\rho_p\sigma_c^3 = 0$, 1, 2 (indicated by arrow); the polymer profile is only shown for $\rho_p\sigma_c^3 = 2$ for clarity.

† As we only deal with z-dependent fluid density profiles in the present study we follow [14, 15] and use the non-tensorial form of the DFT [12].

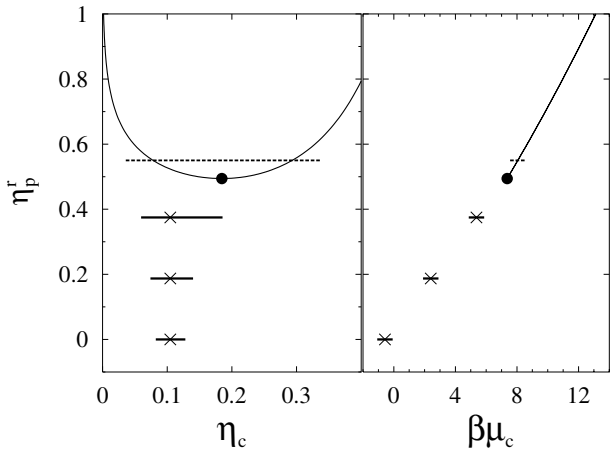

Figure 3. Bulk phase diagram of the AO model for size ratio $q = 0.6$ as a function of polymer reservoir packing fraction η_p^r and colloid packing fraction η_c (left panel) and colloid chemical potential $\beta\mu_c$ (right panel). The vapour–liquid binodal (thin line) and critical point (dot) is shown. Crosses denote the state points where we investigate density profiles. The horizontal bars centred at these state points indicate the variation of the chemical potential along one period of the external field. The dashed bar corresponds to the stacked fluid phase.

not affect directly the polymers, which merely pack in the free space between the colloids. Increasing the polymer concentration leads to an increase of the amplitude of the oscillation in $\rho_c(z)$. Clearly, the minimum and maximum values, defined as

$$\rho_c^{\min} = \min_z \rho_c(z), \quad \rho_c^{\max} = \max_z \rho_c(z), \tag{8}$$

are characteristic measures and we will monitor these below, in particular as a function of λ/σ_c.

Before doing so, we reconsider the bulk phase diagram. In figure 3 we plot the liquid–vapour binodal both as a function of η_c, η_p^r (left panel) and as a function of $\beta\mu_c, \eta_p^r$ (right panel). (In order to fix an arbitrary additive constant to μ_c we use the convention $\Lambda_c = \sigma_c$ in equation (7).) We also indicate the state points where we will carry out detailed structural analysis. In the limit of $\lambda/\sigma_c \to \infty$, a local density approximation is becoming asymptotically exact [34], and hence one can think of locally varying the (bulk) colloid chemical potential. The corresponding variations in μ_c are indicated in figure 3 as horizontal lines. We first examine the (three) cases that are completely inside the one-phase fluid region (hence do not cross the liquid–vapour binodal) and consider the variation with λ while all other parameters (amplitude of the potential, colloid and polymer density and diameters) are kept fixed.

First we consider a pure hard sphere system (i.e. $\eta_p = 0$) with colloid density $\rho_c\sigma_c^3 = 0.2$. In figure 4, results for $\rho_c^{\min}$ and $\rho_c^{\max}$ are plotted as a function of

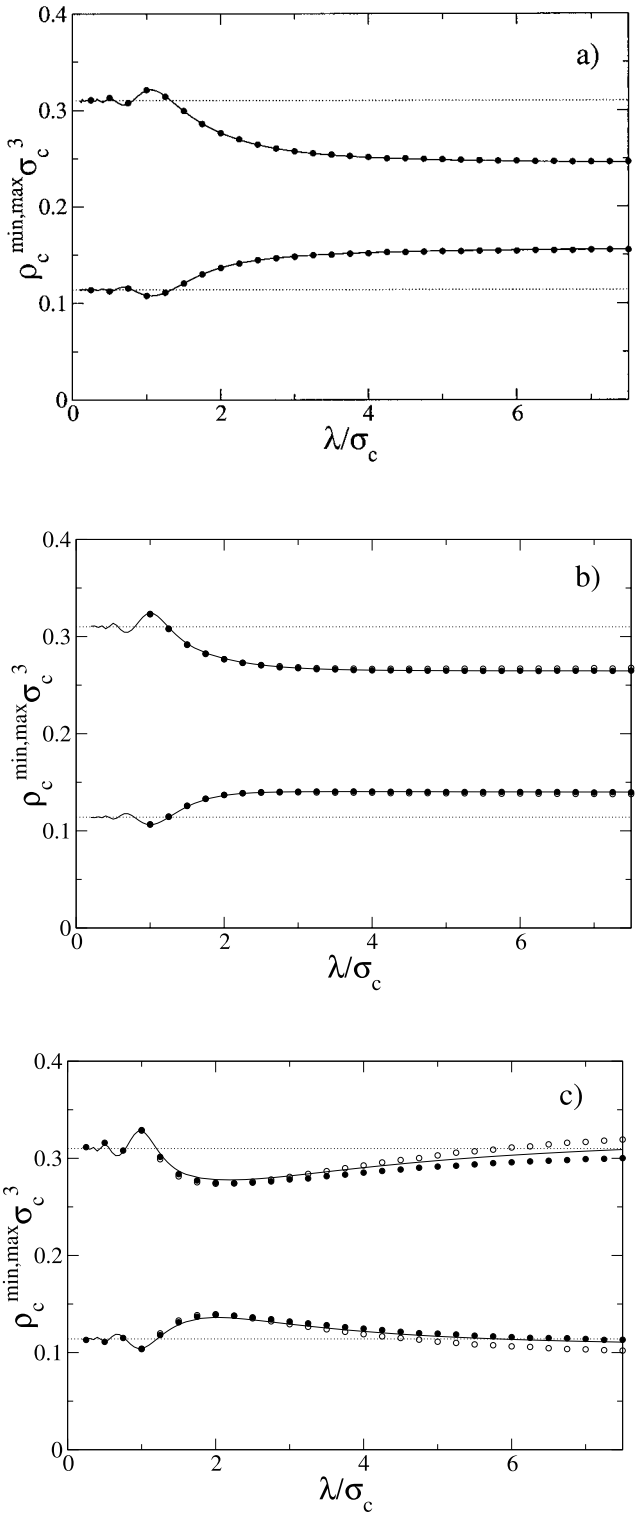

Figure 4. DFT (solid lines) and MC results for the full (filled circles) and effective model (open circles) for the minimum ($\rho_c^{\min}\sigma_c^3$) and maximum ($\rho_c^{\max}\sigma_c^3$) colloid density as a function of the wavelength λ of the external potential for $\rho_c\sigma_c^3 = 0.2$ and different values of ρ_p. The dotted lines represent the result for an ideal gas. (*a*) $\rho_p\sigma_c^3 = 0$ (i.e. pure hard spheres); (*b*) $\rho_p\sigma_c^3 = 1$; (*c*) $\rho_p\sigma_c^3 = 2$.

the (scaled) wavelength λ/σ_c. The DFT results match perfectly those from simulations demonstrating the excellent accuracy of the theory, which equals, in the absence of polymers, Rosenfeld's hard sphere functional.

For $\lambda \approx \sigma_c$ the amplitude of the density oscillation reaches a maximum. This is the case when two colloids *at contact* can be placed in neighbouring minima of the external potential. This leads to very efficient packing of the particles in the valleys of $U_{ext}(z)$. For $\lambda < \sigma_c$ oscillations appear that become smaller in amplitude and in wavelength as $\lambda \to 0$. We attribute this behaviour to the competition of the length scales σ_c and λ. In the limit of very small wavelength, i.e. $\lambda/\sigma_c \to 0$, an exactly solvable case is recovered. Since there are no hard sphere interactions when a particle moves over a length λ, mainly single-particle motion in an external field occurs. The corresponding density profile in this limit is

$$\rho_c(z) = \Lambda_c^{-3} \exp(-\beta[U_{ext}(z) - \mu_c]). \quad (9)$$

Hence $\rho_c^{min} = \Lambda_c^{-3} \exp(-\beta U_0 - \mu_c)$ and $\rho_c^{max} = \Lambda_c^{-3} \exp(\beta U_0 - \mu_c)$. This limit is shown in figure 4 as a dotted line.

For long wavelengths, on the other hand, the maximum density is lower than in the ideal gas case due to the repulsion of the hard spheres. It is decreasing, in general, with increasing λ. This can be understood intuitively as follows. A hard sphere system reacts with marked density oscillations to the presence of an external potential. The amplitude of the density response depends on the range of the external potential; if it is of the order of σ_c the density oscillations are most pronounced while for smooth and longer ranged external potentials the oscillations are weaker. For large λ/σ_c the above mentioned local density approximation holds, and ρ_c^{min}, ρ_c^{max} correspond to the end points of the paths indicated in figure 3.

In figure 4(*b*), the minimum and maximum colloid densities are plotted as a function of the wavelength for $\rho_p\sigma_c^3 = 1$. Adding polymers, the effective attraction causes a higher maximum density in the potential valleys. As the total density is constant, the minimum density decreases. We show results from the direct simulation of the binary mixture and from the simulation of the one-component model. From the binary simulation we determine $\eta_p^r = 0.18465$, which we use in equation (5). This value for η_p^r is slightly smaller than the free-volume bulk result $\eta_p^r = 0.187376$. We have also checked that η_p^r does not change significantly as λ/σ_c varies. From $\lambda/\sigma_c = 1$–7.5 only a small decrease $\eta_p^r = 0.185$–0.1845 is found, and we are confident that keeping η_p^r fixed is a good approximation. As is apparent in figure 4(*b*), the differences between the binary and the effective models are very small, and we conclude that the higher-body terms neglected in the one-component model do not contribute significantly. Again the DFT gives a very good account of the observed behaviour.

In figure 4(*c*), the results for an even higher polymer concentration, $\rho_p\sigma_c^3 = 2$, are presented. At $\lambda \approx 2\sigma_c$, a minimum in the amplitude occurs and ρ_c^{max} *increases* with increasing λ in striking contrast to the pure hard sphere case. This can be understood in terms of the strong effective attraction which prefers locally higher density and acts oppositely to the correlation effect discussed above for pure hard spheres. Figure 4(*b*) is an intermediate case where the effective attraction is not strong enough to lead to increasing ρ_c^{max} with increasing λ.

For the simulation of the effective one-component system we use the simulated value $\eta_p^r = 0.365$. This was determined for small wavelengths (the free-volume result in bulk is $\eta_p^r = 0.374735$). In reality η_p^r decreases, but only very little with increasing λ/σ_c; we estimate $\eta_p^r = 0.363$ for $\lambda/\sigma_c = 7.5$. From figure 4(*c*), one sees that in the effective model the effect of the polymers is overestimated. We attribute this mainly to the fact that the (repulsive) three-body forces are neglected. The DFT still describes the simulation results quite well, although the agreement is slighlty inferior to the above cases.

Finally, we show results for $0.25 < \lambda/\sigma_c < 1.25$ on an expanded scale in figure 5. The damping and increasing of wavelength of oscillations as λ/σ_c decreases is apparent. The presence of the polymers shifts the absolute maximum (minimum) of ρ_c^{max} (ρ_c^{min}) to smaller λ_c/σ_c. Having gained confidence in the theory, in the

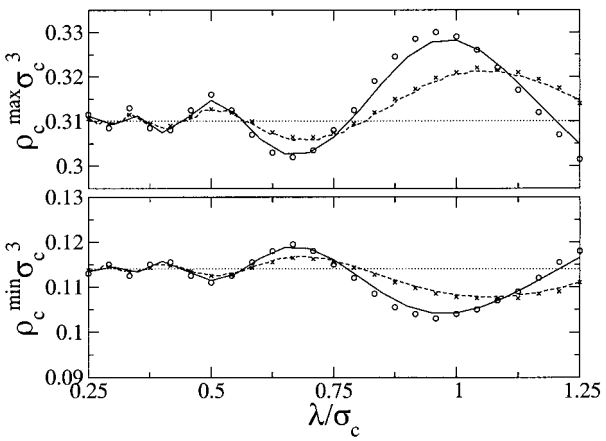

Figure 5. Same as figure 4, but for $0.25 < \lambda/\sigma_c < 1.25$. Lines are DFT results, symbols denote computer simulation results. The hard sphere case for $\rho_p = 0$ (dashed line and crosses) and $\rho_p\sigma_c = 2$ (solid line and open circles) are shown; results for $\rho_c\sigma_p^3 = 1$ are omitted for clarity.

following we investigate the effect of increased polymer density so that demixing occurs.

5.2. *Phase behaviour*

In order to study the fluid demixing phase behaviour we use the same parameters as before, i.e. $q = 0.6$ and $\beta U_0 = 0.5$. We restrict ourselves to $\lambda = 8.192\sigma_c$, where we show detailed results, but we have also considered smaller λ to assess the principal scenario. In figure 6 the phase diagram as obtained from DFT is shown. For large η_p^r the presence of the plane wave potential shifts the bulk transition slightly to higher colloid chemical potentials $\beta\mu_c$. Strikingly however, at lower η_p^r values a bifurcation of the binodal occurs. It appears that the two bifurcated critical points lie at the same η_p^r value as the bulk critical point but numerically we could not determine whether they are exactly the same. Three state points are indicated where we plot the density profiles in figure 7, one in each region. The three state points are all at $\eta_p^r = 0.65$ and (i) modulated gas, $\beta\mu_c = 8.7$, (ii) stacked fluid, $\beta\mu_c = 9.2$ and (iii) modulated liquid, $\beta\mu_c = 9.7$. The stacked fluid phase is a novel phase which is absent in the bulk but is stabilized by the external field. It consists of periodic slabs of vapour centred around the maxima of the external potential and of slabs of liquid centred around the minima of the external potential. The relative width of the vapour and liquid portion do vary with the thermodynamic parameters. The occurrence of the stacked fluid phase is most directly understood in the limit $\lambda/\sigma_c \to \infty$ where

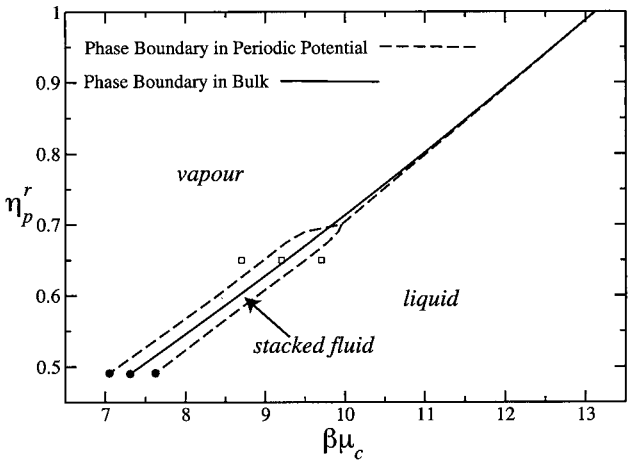

Figure 6. Fluid demixing phase diagram of the AO model as a function of colloid chemical potential $\beta\mu_c$ and polymer reservoir packing fraction η_p^r for size ratio $q = 0.6$ for the cases without external potential (solid line) and with external potential of strength $\beta U_0 = 0.5$ and wavelength $\lambda = 8.192\sigma_c$. In the latter case three phases (vapour, stacked fluid, liquid) are observed. Solid symbols denote critical points. Open symbols denote state points where we display density profiles in figure 6.

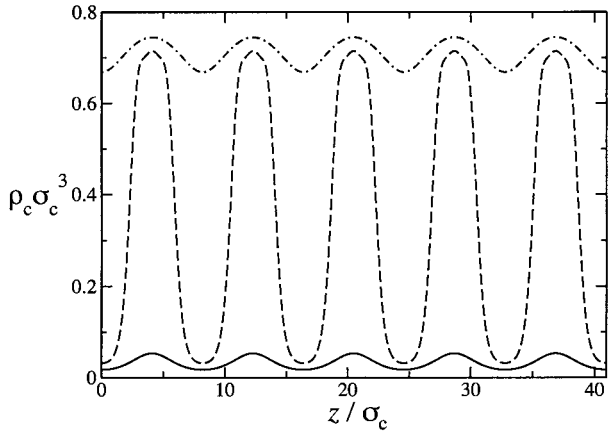

Figure 7. Colloid density profiles for $\beta U_0 = 0.5$, $\lambda = 8.192\sigma_c$, $q = 0.6$ and $\eta_p^r = 0.65$ in three different phases corresponding to different chemical potentials: modulated vapour for $\beta\mu_c = 8.7$ (solid line), stacked fluid for $\beta\mu_c = 9.2$ (dashed line) and modulated liquid for $\beta\mu_c = 9.7$ (dot-dashed line).

a local density approximation is valid. When the combination $\mu_c - U_{ext}(z)$ equals the chemical potential at liquid–vapour coexistence (see the dashed bar in the right panel of figure 3) a liquid–vapour interface is built up [34].

For smaller values of λ/σ_c we have confirmed that the stacked fluid ceases to exist and the usual type of vapour–liquid phase diagram is recovered. The disappearance is due to the increasing contribution of surface free energy between liquid and vapour slabs in the stacked phase as λ is decreased. We have checked that eventually, at a *finite* value of λ/σ_c, the stacked fluid is no longer stable. Upon decreasing λ/σ_c the triple point moves toward both critical points eventually merging in a bicritical point. We leave a more thorough study of the details of this scenario to possible future work.

6. Conclusions

We have considered a model colloid–polymer mixture exposed to a three-dimensional plane wave external potential representing an optical standing wave. By tuning the size and concentration of the polymers, one can influence the range and strength of an effective depletion attraction, and this can be adjusted so that stable colloid vapour–liquid coexistence is observed.

We have demonstrated that a recent DFT quantitatively predicts the inhomogeneous density profiles when compared to simulation results. As a function of the wavelength of the external potential we find interesting, non-monotonic behaviour of the amplitude of the oscillations in the one-body density distributions. Furthermore we demonstrate the stability of a stacked liquid phase. All our predictions can in principle be verified

in experiments of colloid–polymer mixtures. We believe that the trends and the appearance of the stacked fluid phase are very general phenomena which should also be present for more realistic polymer–polymer and colloid–polymer interactions [35].

Motivated by the experimental situation, in our study the external potential acts only on the colloids. It might, however, also be interesting to study external potentials that act solely or differently on the polymers. In the depletion picture this would lead to spatially varying pair potentials—an interesting issue.

In order to realize small λ/σ_c one needs to use core-shell colloidal particles, where the laser only couples to the particle core.

The principal physical mechanism that underlies the stability of the stacked fluid should also apply to two-dimensional systems; these might be easier to access experimentally.

Finally we note that an analogue of the stacked fluid phase was found before in parallel slit pores where the confining walls are periodically structured. The familiar capillary condensation from gas to liquid is enriched in this case by a phase that consists of liquid bridges between both walls [36, 37]. This phase was also obtained within a lattice model between decorated walls [38]. We emphasize, however, that our external potential is simpler as it has only two additional control parameters such that in our situation the occurrence of the intermediate fluid phase is more direct.

The work of JMB was supported by the National Science Foundation (through grant CHE9800074 and the NSF Materials Research Science and Engineering Center at the University of Chicago). MS and HL acknowledge support from the DFG through the SFB TR6.

References

[1] Asakura, S., and Oosawa, F., 1958, *J. polym. Sci.*, **33,** 183.
[2] Vrij, A., 1976, *Pure appl. Chem.*, **48,** 471.
[3] Pusey, P. N., 1991, *Liquids, Freezing and the Glass Transition*, edited by J. P. Hansen, J. Zinn-Justin, and D. Levesque (Amsterdam: North Holland).
[4] Dijkstra, M., van Roij, R., and Evans, R., 2000, *J. chem. Phys.,* **113,** 4799; Brader, J. M., and Evans, R., 2000, *Europhys. Lett.*, **49,** 678; Brader, J. M., Dijkstra, M., and Evans, R., 2001, *Phys. Rev.* E, **63,** 041405.
[5] Likos, C. N., 2001, *Phys. Rep.*, **348,** 267.
[6] Hansen, J. P., and Löwen, H., 2003, *Effective Interactions for Large-scale Simulations of Complex Fluids, Springer Series*, edited by P. Nielaba, M. Mareschal, and G. Ciccotti (Berlin: Springer).
[7] Anderson, V. J., and Lekkerkerker, H. N. W., 2002, *Nature*, **416,** 811.
[8] Fuchs, M., and Schweizer, K. S., 2002, *J. Phys.: condens. Matter*, **14,** R239.
[9] Poon, W. C. K., 2002, *J. Phys.: condens. Matter*, **14,** R859.
[10] Löwen, H., 2001, *J. Phys.: condens. Matter*, **13,** R415.
[11] Rosenfeld, Y., 1989, *Phys. Rev. Lett.*, **63,** 980.
[12] Schmidt, M., Löwen, H., Brader, J. M., and Evans, R., 2000, *Phys. Rev. Lett.*, **85,** 1934.
[13] Schmidt, M., Löwen, H., Brader, J. M., and Evans, R., 2002, *J. Phys.: condens. Matter*, **14,** 9353.
[14] Evans, R., Brader, J. M., Roth, R., Dijkstra, M., Schmidt, M., and Löwen, H., 2001, *Phil. Trans. R. Soc.* (London) A, **359,** 961.
[15] Brader, J. M., Evans, R., Schmidt, M., and Löwen, H., 2002, *J. Phys.: condens. Matter*, **14,** L1.
[16] Dijkstra, M., and van Roij, R., 2002, *Phys. Rev. Lett.* , **89,** 208303.
[17] Aarts, D. G. A L., van der Wiel, J. H., and Lekkerkerker, H. N. W., 2003, *J. Phys.: condens. Matter*, **15,** S245.
[18] Wijting, W. K., Besseling, N. A. M., and Cohen Stuart, M. A., unpublished.
[19] Bechinger, C., Wei, Q. H., and Leiderer, P., 2000, *J. Phys.: condens. Matter*, **12,** A425.
[20] Wei, Q. H., Bechinger, C., Rudhardt, D., and Leiderer, P., 1998, *Phys. Rev. Lett.*, **81,** 2606.
[21] Loudiyi, K., and Ackerson, B. J., 1992, *Physica* A, **184,** 1.
[22] Chowdhury, A., Ackerson, B. J., and Clark, N. A., 1985, *Phys. Rev. Lett.*, **55,** 833.
[23] Loudiyi, K., and Ackerson, B. J., 1992, *Physica* A, **184,** 26.
[24] Chakrabarti, J., Krishnamurthy, H. R., Sood, A. K., and Sengupta, S., 1995, *Phys. Rev. Lett.*, **75,** 2232.
[25] Strepp, W., Sengupta, S., and Nielaba, P., 2001, *Phys. Rev.* E, **63,** 046106.
[26] Barrat, J. L., and Xu, H., 1990, *J. Phys.: condens. Matter*, **2,** 9445.
[27] Chakrabarti, J., Krishnamurthy, H. R., and Sood, A. K., 1994, *Phys. Rev. Lett.*, **73,** 2923.
[28] Rasmussen, L. L., and Oxtoby, D. W., 2002, *J. Phys.: condens. Matter*, **14,** 12021.
[29] Frey, E., Nelson, D. R., and Radzihovsky, L., 1999, *Phys. Rev. Lett.*, **83,** 2977.
[30] Das, C., Sood, A. K., and Krishnamurthy, H. R., 1999, *Physica* A, **270,** 237.
[31] Lekkerkerker, H. N. W., Poon, W. C. K., Pusey, P. N., Stroobants, A., and Warren, P. B., 1992, *Europhys. Lett.*, **20,** 559.
[32] Bolhuis, P. G., Louis, A. A., and Hansen, J. P., 2002, *Phys. Rev. Lett.*, **89,** 128302.
[33] Dijkstra, M., Brader, J. M., and Evans, R., 1999, *J. Phys.: condens. Matter*, **11,** 10079.
[34] See e.g. Dzubiella, J., Harreis, H. M., Likos, C. N., and Löwen, H. L., 2001, *Phys. Rev.* E, **64,** 011405.
[35] Jusufi, A., Dzubiella, J., Likos, C. N., von Ferber, C., and Löwen, H., 2001, *J. Phys.: condens. Matter*, **13,** 6177.
[36] Schoen, M., and Diestler, D. J., 1997, *Phys. Rev.* E, **56,** 4427.
[37] Röcken, P., Somoza, A., Tarazona, P., and Findenegg, G., 1998, *J. chem. Phys.*, **108,** 8689.
[38] Beck, H., Diestler, D. J., and Schoen, M., 2001, *J. Phys.: condens. Matter*, **13,** 4697.